The Journal of Neuroscience, April 15, 2002, 22(8):3033–3043

Odorant Receptor Expression Defines Functional Units in the Mouse Olfactory System

Thomas Bozza, Paul Feinstein, Chen Zheng, and Peter Mombaerts

The Rockefeller University, New York, New York 10021

Odorant receptors (ORs) mediate the interaction of odorous compounds with olfactory sensory neurons (OSNs) and influence the guidance of OSN axons to synaptic targets in the olfactory bulb (OB). OSNs expressing the same OR send convergent axonal projections to defined glomeruli in the OB and are thought to share the same odorant response properties. This expectation of functional similarity has not been tested experimentally, because it has not been possible to determine reproducibly the response properties of OSNs that express defined ORs. Here, we applied calcium imaging to characterize the odorant response properties of single neurons from gene-targeted mice in which the green fluorescent protein is coexpressed with a particular OR. We show that the odorants acetophenone and benzaldehyde are agonists for the M71 OR and that M71-expressing neurons are functionally similar in their response properties across concentration. Replacing the M71 coding sequence with that of the rat I7 OR changes the stimulus response profiles of this genetically defined OSN population and concomitantly results in the formation of novel glomeruli in the OB. We further show that the mouse I7 OR imparts a particular response profile to OSNs regardless of the epithelial zone of expression. Our data provide evidence that ORs determine both odorant specificity and axonal convergence and thus direct functionally similar afferents to form particular glomeruli. They confirm and extend the notion that OR expression provides a molecular basis for the formation and arrangement of glomerular functional units.

Key words: olfaction; olfactory system; olfactory bulb; glomerulus; sensory neuron; olfactory receptor; odorant receptor; calcium imaging; green fluorescent protein

The olfactory system provides mammals with the ability to perceive a large number of structurally diverse odorous molecules, often at minute concentrations, and to discriminate subtle differences in molecular structure. Chemical properties of odorants are represented as spatiotemporal patterns of activity across olfactory sensory neurons (OSNs) in the olfactory epithelium. Each OSN has a single dendrite terminating in olfactory cilia that extend into the lumen of the nasal cavity. In vertebrates, odorant transduction is mediated by G-protein-coupled receptors, which are encoded by a family of ~1000 odorant receptor (OR) genes in mouse (Buck and Axel, 1991; Mombaerts, 1999; Zhang and Firestein, 2002). Mouse OSNs likely express a single member from this OR repertoire (Malnic et al., 1999).

Whereas a given OR is expressed by neurons scattered in broad zones of the olfactory epithelium (Ressler et al., 1993; Vassar et al., 1993), the axons from OSNs that express the same OR converge onto defined glomeruli in the olfactory bulb (OB) (Ressler et al., 1994; Vassar et al., 1994; Mombaerts et al., 1996). Olfactory glomeruli are spherical regions of neuropil in which olfactory afferents synapse with the dendrites of output and intrinsic neurons of the OB. In vertebrates, a variety of functional techniques have shown that individual odorants elicit distributed but reproducible spatiotemporal patterns of glomerular activation (Kauer and Cinelli, 1993; Friedrich and Korsching, 1997; Johnson et al., 1999; Rubin and Katz, 1999). These data support the widely held view that glomeruli are functional units in olfactory processing (Kauer and Cinelli, 1993; Hildebrand and Shepherd, 1997; Mori et al., 1999). The glomerular convergence of afferents that express a given OR strongly suggests that glomeruli integrate inputs from OSNs that share similar odorant response profiles (Kauer, 1987).

Several approaches have associated odorous agonists with particular mammalian ORs (Krautwurst et al., 1998; Zhao et al., 1998; Malnic et al., 1999; Murrell and Hunter, 1999; Touhara et al., 1999; Araneda et al., 2000; Kajiya et al., 2001). However, the functional similarity of OSNs that express the same OR from an endogenous locus have not been examined. Here, we report the analysis of odorant response properties from genetically identified OSNs that express particular OR genes and that send convergent axonal projections to defined glomeruli. Our results reveal consistent odorant response profiles in neurons expressing a defined OR. Replacing the OR at a genetic locus changes odorant responsiveness and concomitantly shifts the site of axonal convergence. In contrast, a given OR imparts the same odorant response profile when expressed in different epithelial zones from distinct OR loci. Our data provide evidence that expression of a given OR is sufficient to direct the formation of glomeruli from functionally similar olfactory afferents.

Received Nov. 26, 2001; revised Jan. 25, 2002; accepted Feb. 5, 2002.

T.B, P.F., and C.Z. were supported by postdoctoral fellowships from the National Institutes of Health. P.M. acknowledges support from the National Institutes of Health and the Human Frontier Science Program and was an Alfred P. Sloan, Basil O'Connor, Guggenheim, Irma T. Hirschl, Klingenstein, McKnight, Rita Allen, and Searle Scholar Fellow. We thank Annemarie Walsh and Ruben Peraza from the Transgenic Service at The Rockefeller University for generating chimeric mice and Mario Capecchi for providing the ACN plasmid. Special thanks to Kathleen Dorries and Ivan Rodriguez for providing critical comments on this manuscript.

Correspondence should be addressed to Peter Mombaerts, The Rockefeller University, 1230 York Avenue, New York, NY 10021. E-mail: peter@rockefeller.edu.

 0270-6474/02/223033-11$15.00/0

MATERIALS AND METHODS

Gene targeting. The mouse *I7* and *M71* targeting vectors were derived from genomic fragments isolated from a mouse (129/Sv) λ FixII library (Stratagene, La Jolla, CA). A fragment of the *M71* OR gene (Ressler et al., 1993; Xie et al., 2000) was isolated by PCR and used as a probe. A 9.2 kb fragment containing *M71* was subcloned in pBS-SK, and a *Pac*I site

was engineered three nucleotides downstream of the stop codon by recombinant PCR, creating the plasmid *M71/Pac*. A cassette containing *IRES-tauGFP-LTNL* (Rodriguez et al., 1999) was inserted into the *Pac*I site of *M71/Pac*, yielding the *M71-IRES-tauGFP-LTNL* targeting vector.

For OR swaps, the *M71* coding sequence was replaced exactly from the start codon to the stop codon with the rat and mouse *I7* coding sequences without the insertion of linker sequences or extraneous nucleotides. The coding sequence of the rat *I7* OR gene (Buck and Axel, 1991) was isolated by PCR from an adenovirus vector (Ad-I7) (Zhao et al., 1998), cloned, and sequenced. For the rI7→M71 targeted mutation, the *IRES-GFP-IRES-taulacZ* sequence was inserted as a cassette, along with *pgk-neo* flanked by loxP sites (Rodriguez et al., 1999). For the mI7→M71 targeted mutation, a cassette containing a self-excising *pgk-neo* gene, ACN (Bunting et al., 1999), and *IRES-tauGFP* sequences (*ires-tauGFP-ACNF*) was inserted into the *Pac*I site. For mouse I7, a 7.1 kb fragment containing the *I7* coding sequence was subcloned into pBS-KS and engineered with a *Pac*I site three nucleotides downstream of the stop codon, into which was inserted the *IRES-tauGFP-ACNF* cassette.

Targeting vectors were linearized with *Pme*I and electroporated into E14 embryonic stem (ES) cells as described previously (Mombaerts et al., 1996). Genomic DNA from G418-resistant ES clones was analyzed by Southern blot hybridization with probes external to the targeting vectors. For the M71-G mutation (ES clone A43/Cre14), the selectable markers were removed through Cre recombinase-mediated recombination in ES cells, using negative selection with ganciclovir to select against expression of HSV-tk (Mombaerts et al., 1996). For the rI7→M71-G mutation (ES clone IMGT49), the *neo*-selectable marker was removed *in vivo* by crossing heterozygous mice to EIIa-Cre transgenic mice (Lakso et al., 1996). Interbreeding mice with the recombined loxP allele produced a line that was homozygous for the targeted mutation and negative for the Cre transgene. For mI7-G and mI7→M71-G strains (ES clones I7TG186 and I7M7150), germline excision of the *neo* cassette and transmission of the loxP alleles were confirmed by PCR analysis in F1 progeny. Mice are in a mixed (129 × C57BL/6J) background.

Whole-mount analysis. Unfixed epithelial whole mounts were imaged using a confocal microscope (LSM-510; Zeiss, Oberkochen, Germany). Whole mounts of the OB were viewed using a Zeiss SV11 fluorescence stereomicroscope with a cooled CCD camera (SensiCam; Cooke Corporation, Auburn Hills, MI).

Cell dissociation and calcium imaging. Two to 3-week-old mice were used for physiological experiments. Isolation of mouse OSNs and loading with fura-2 AM were performed as described previously (Bozza and Kauer, 1998). Ratiometric calcium imaging (340 and 380 nm excitation) was performed using an inverted microscope (Diaphot; Nikon, Tokyo, Japan) equipped with a 40×, 1.3 numerical aperture objective, a filter wheel (Sutter Instruments, Novato, CA), and a 75 W xenon lamp attenuated with neutral density filters. OSNs were identified by bright-green fluorescence and by the presence of an intact dendrite and cilia. Green fluorescent protein (GFP) and fura-2 fluorescence could be separated using appropriate filters (GFP, 475DF40 excitation, 505LP dichroic, 535/50 emission; fura-2, 340HT15 and 380HT15 excitation, 430DCLP dichroic, 470EFLP emission; Omega Optical, Brattleboro, VT). Images were acquired using a cooled CCD camera (SensiCam; Cooke Corporation); image frames (640 × 512 pixels) were integrated for 80 msec and binned 2 × 2. Ratio image pairs were acquired at 0.5 Hz during stimulus delivery and 0.25 Hz between stimuli; ratios were calculated from the average pixel values over OSN cell bodies after background subtraction. Filter wheel control and image acquisition were performed using Metafluor 4.0 (Universal Imaging Corporation, West Chester, PA).

Only OSNs that responded to high K^+ Ringer's solution (100 mM KCl) were analyzed. Brief pulses of 500 μM 3-isobutyl-1-methylxanthine (IBMX) did not consistently induce somatic calcium changes in odorant responsive mouse OSNs. In contrast, 10 μM forskolin always elicited a short-latency Ca^{2+} response in odorant-responsive OSNs but was ineffective in neurons that lacked cilia (data not shown), did not respond to odorants, or were deficient in an olfactory cyclic nucleotide-gated channel subunit (Zheng et al., 2000). All odorant responses were repeated at least once. Replicate response amplitudes were averaged, or, in cases in which response amplitude ran down over time, the largest response to a particular stimulus was included. The size of the dots in the dot plots is proportional to the amplitude of the calcium response to an odorant at the given concentration, relative to the amplitude of the response to KCl in the same neuron. For the plots, a threshold of 1% (or approximately one SD from baseline across cells) is set for the smallest dot.

All dose–response data were derived from estimates of absolute $[Ca^{2+}]_i$ determined from *in situ* calibrations within cells using standard methods (Grynkiewicz et al., 1985; Kao, 1994). The relationship between the normalized $[Ca^{2+}]_i$ response amplitudes, R, and odorant concentration, C, was fitted by the Hill equation $R = 1/[1 + (EC_{50}/C)^n]$ to obtain EC_{50} values.

Odorants were of the highest purity available (≥98% pure) and were purchased from Fluka (Neu-Ulm, Germany), Sigma (St. Louis, MO), and Aldrich (Milwaukee, WI) or were gifts from Givaudan Roure (Dübendorf, Switzerland). Individual odorants and mixtures were made up as 1 mM stocks and diluted to a final working concentration in Ringer's solution. IBMX and forskolin (Sigma) were prepared as 50 and 500 mM stocks, respectively, in DMSO and diluted in Ringer's solution. Stimuli were bath applied in 4 sec pulses using a gravity-fed superfusion system.

RESULTS

Gene targeting at the *M71* locus

The M71 OR (Ressler et al., 1993; Xie et al., 2000) was chosen for functional analysis because axons of M71-expressing OSNs project to glomeruli in the dorsal OB, a region that is amenable to future anatomical and physiological analysis *in vivo*. The M71 OR is a close homolog of M72 (Zheng et al., 2000). Previous *in situ* hybridization studies had shown that a *M71* probe labels a small subset of glomeruli in the dorsal OB (Ressler et al., 1993).

To vitally label *M71*-expressing OSNs (M71 OSNs), we generated a strain of mice using gene targeting in which an internal ribosome entry site (*IRES*) and the coding sequence for the fluorescent, axonal marker tauGFP (Rodriguez et al., 1999) were inserted downstream of the *M71* coding sequence, producing the *M71-IRES-tauGFP* (M71-G) mutation (Fig. 1*A*). In these mice, neurons that express the *M71* locus transcribe a bicistronic mRNA, allowing for the translation of the tauGFP marker without altering the *M71* coding sequence. Expression of tauGFP from the *M71* locus results in bright green fluorescence in neuronal cell bodies distributed throughout the dorsal zone of the olfactory epithelium (Fig. 1*B*).

To correlate an odorant-response phenotype with a particular OR coding sequence, a receptor "swap" was generated by gene targeting in which the rat *I7* coding sequence replaces the mouse *M71* coding sequence at the *M71* locus (rI7→M71) (Fig. 1*A*). Consequently, OSNs that transcribe this modified *M71* allele (rI7→M71 OSNs) express the rat I7 OR instead of the mouse M71 OR; this is also the case in mice heterozygous for the mutation as a result of monoallelic expression (Chess et al., 1994; Strotmann et al., 2000). Rat I7 was chosen because its response profile has been characterized in great detail (Krautwurst et al., 1998; Zhao et al., 1998; Wetzel et al., 1999; Araneda et al., 2000), but its response profile has not been thoroughly examined in individual OSNs. To label neurons expressing the rI7→M71 allele, *IRES-GFP* and *IRES-taulacZ* were appended immediately after the rat *I7* coding sequence, producing the *rI7→M71-IRES-GFP-IRES-taulacZ* (rI7→M71-G) mutation (Fig. 1*A*). The double *IRES* construct results in the translation of two separate markers, along with the OR from a tricistronic mRNA (Zheng et al., 2000). This allows the identification of rI7→M71 OSNs and axons by intrinsic GFP fluorescence and the discrimination of these cells from M71 OSNs by 5-bromo-4-chloro-3-indolyl-β-D-galactopyranoside (X-gal) staining for β-galactosidase activity. In this mouse strain, the zonal distribution of GFP-labeled neurons is the same as observed in M71-G mice, indicating that the expression pattern of the *M71* locus is preserved (Fig. 1*C*).

Imaging of vitally labeled OSNs

Odorant responsiveness of GFP-labeled OSNs was measured using fura-2 calcium imaging in single cells; calcium imaging has

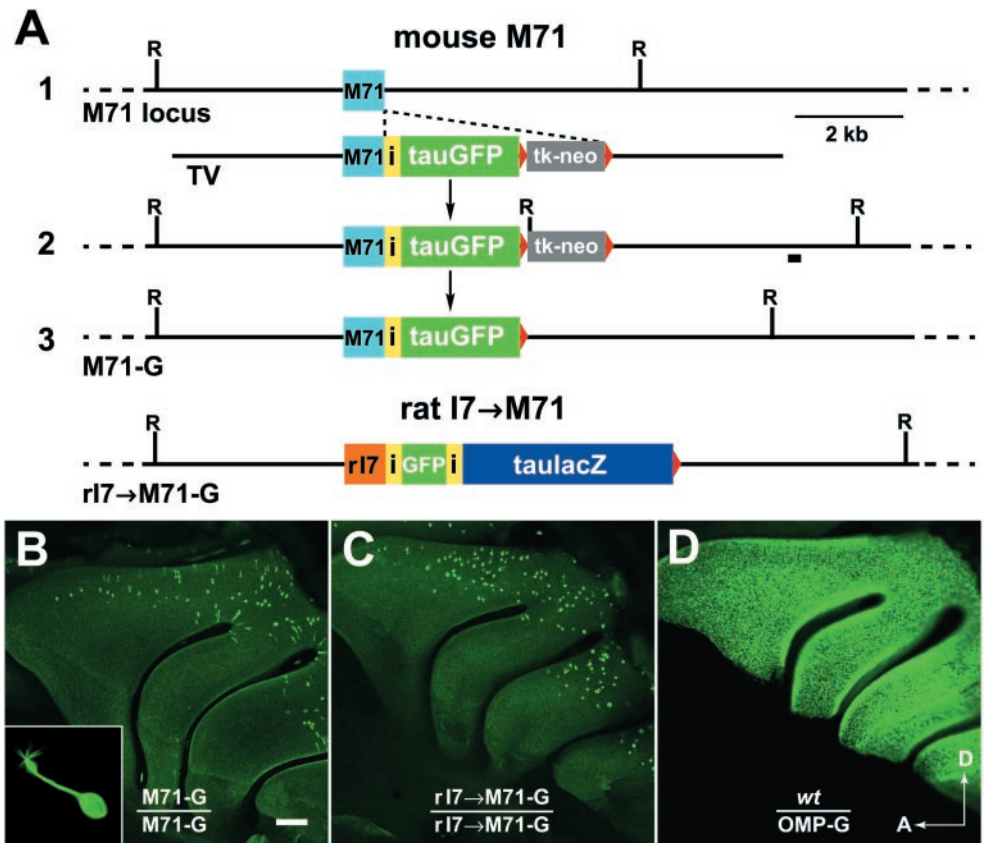

Figure 1. Vital labeling of M71 and rI7→M71 OSNs. *A*, Wild-type *M71* OR locus (*1*) showing the unmodified *M71* coding sequence (*light blue box*) is shown with the *M71-IRES-tauGFP* targeting vector (*TV*). Relevant restriction sites are indicated (*R*, *Eco*RI). The *M71* coding sequence is followed immediately after the stop codon by the *IRES* (*yellow box*) and the *tauGFP* coding sequence (*green box*), thus encoding a biscistronic message. The negative selectable marker *HSV-tk* followed by the positive selectable marker *pgk-neo* (*gray box*) are flanked by loxP sites (*red triangles*). The M71-G allele results from homologous recombination (*2*) and Cre-mediated excision of the selectable marker (*3*), leaving a single loxP site. The *black box* on the *right* represents the 3′ external probe used to identify homologous recombination by Southern blot hybridization. Swap of the rat *I7* coding sequence (*orange box*) into the *M71* locus in which the *M71* coding sequence is replaced with that of rat *I7*. Both *IRES-GFP* and *IRES-taulacZ* are placed immediately downstream, thus encoding a tricistronic message. *B*, View of the medial turbinates in an epithelial whole mount from a homozygous M71-G mouse. tauGFP-labeled OSNs (*bright green*) are found in the dorsal, caudal epithelium (zone 4). Background autofluorescence reveals the overall structure of the turbinates. *Inset*, Fluorescence image of a single tauGFP-labeled M71 OSN taken after calcium recording. Note robust fluorescence in the cell body (*bottom right*), dendrite, and olfactory cilia (*top left*). *C*, Medial view of the turbinates in a homozygous rI7→M71-G mouse showing a similar pattern of GFP-labeled OSNs in the dorsalmost zone of the epithelium (zone 4). *D*, For comparison, all mature OSNs are labeled with GFP in an OMP-GFP mouse (Potter et al., 2001), revealing all epithelial zones. Autofluorescence in the respiratory epithelium is not visible because the exposure was adjusted for the intense GFP fluorescence from the sensory epithelium. *A*, Anterior; *D*, dorsal. Scale bar: *B*, *C*, *D*, 250 μm; *inset in B*, 12 μm.

been used extensively to study odorant responses in olfactory neurons from a variety of species (Schild and Restrepo, 1998). Odorants were initially presented as a set of six mixtures comprising 48 compounds (Fig. 2, *Mix A–Mix F*) to increase the probability of finding an adequate stimulus for uncharacterized ORs. This approach was first established using dissociated cells from OMP-GFP mice (Potter et al., 2001), in which the *OMP* (olfactory marker protein) coding sequence is replaced with the coding sequence for *GFP*, resulting in robust fluorescent labeling of all mature OSNs (Fig. 1*D*). These experiments served to characterize the baseline response profiles to the odorant mixtures for a random sample of neurons that expresses the entire repertoire of ORs. OMP-GFP heterozygous mice were used to avoid adverse physiological effects of the absence of OMP (Buiakova et al., 1996). The viability of labeled OSNs was assessed by KCl depolarization.

Of 121 KCl-responsive OSNs from 15 mice, 22 (18%) responded to at least one odorant mixture (Fig. 3*A*,*B*, *cells 1–22*). The proportion of responsive cells, as well as the time course and amplitudes of the responses, are similar to those seen in previous studies (Bozza and Kauer, 1998).

Odorant response profiles from OMP-GFP OSNs varied in selectivity and breadth of tuning, with neurons responding to as few as one and as many as five mixtures (Fig. 3*B*). The proportion of neurons that responded to different chemical classes of odorants varied considerably. Mix C, a set of aromatic terpenoids, and mix D, a set of aliphatic and aromatic aldehydes, were the most effective stimuli, because 20 of 22 responsive neurons were stimulated by one or both of these mixtures. Three of nine (33%) mix D-responsive cells responded to octanal, a reported agonist for rat I7 (Krautwurst et al., 1998; Zhao et al., 1998). Mixes B, E, and F, which comprise mainly organic acids, alcohols, esters, and ketones, were much less effective at the single concentration tested. Thus, the odorant mixtures reveal the functional diversity that would be expected from OSNs expressing many distinct ORs, providing an important control for the next series of experiments.

Functional similarity among M71 OSNs

We next screened for effective stimuli and characterized the response profiles of M71 OSNs. Variation in odorant response profiles could appear as differences in the subset of odorants to which cells respond or in a proportion of cells that fail to respond to the stimulus set. However, failure to respond could also indicate that a neuron lacks an intact odorant transduction pathway. To rule out the latter possibility, OSNs were tested with the phosphodiesterase inhibitor IBMX and the adenylyl cyclase activator forskolin (Frings and Lindemann, 1991; Leinders-Zufall et al., 1997; Wong et al., 2000) (see Materials and Methods). The tauGFP marker brightly labels cilia (Fig. 1*B*, *inset*), facilitating the unambiguous identification of intact neurons that retain cilia *in vitro*. This spatial distribution of tauGFP is expected if the tau domain mediates association of the marker with microtubules (Brand, 1995).

To screen for agonists and to define a preliminary response

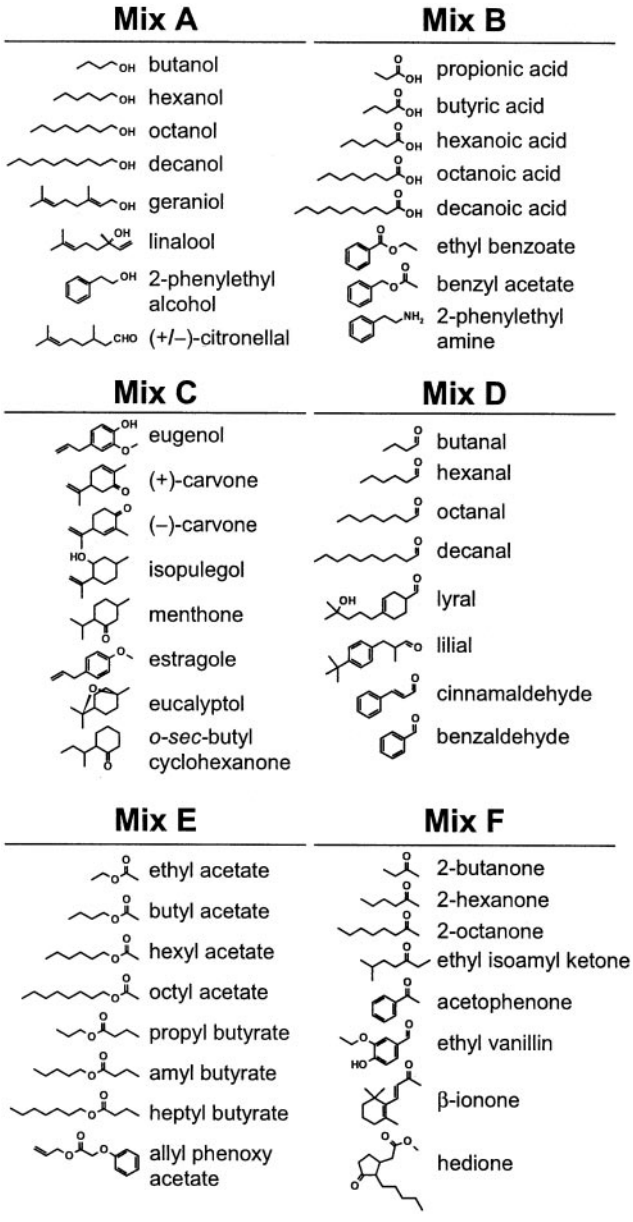

Figure 2. Chemical structures of odorant stimuli. The odorant stimulus set consists of 48 compounds divided into six mixtures (*Mix A–Mix F*) comprising several homologous series, including normal aliphatic and terpene alcohols, organic acids, aldehydes, esters, and ketones, as well as cyclic terpenoids and related compounds.

profile for M71 OSNs, 30 KCl-responsive neurons from 32 mice were tested with the odorant mixtures. Of 16 forskolin-responsive neurons, 14 responded to at least one of the mixtures. Of these, 12 neurons were held long enough to repeat all odorant presentations and were thus included in the analysis (Fig. 3*B*, *cells 1–22*). All 12 M71 OSNs responded to mix F, and four (33%) also exhibited a response of equal or smaller amplitude to mix D at the same concentration. Compared with our random sample of OMP-GFP OSNs, in which responses to mix F were infrequent (4 of 22 neurons; 18%), M71 OSNs responded to a restricted subset of odorant mixtures.

Next, profiles for individual compounds were characterized by testing a second set of 17 KCl-responsive neurons from 30 mice to components of mix F and mix D (Fig. 4). Of 13 forskolin-

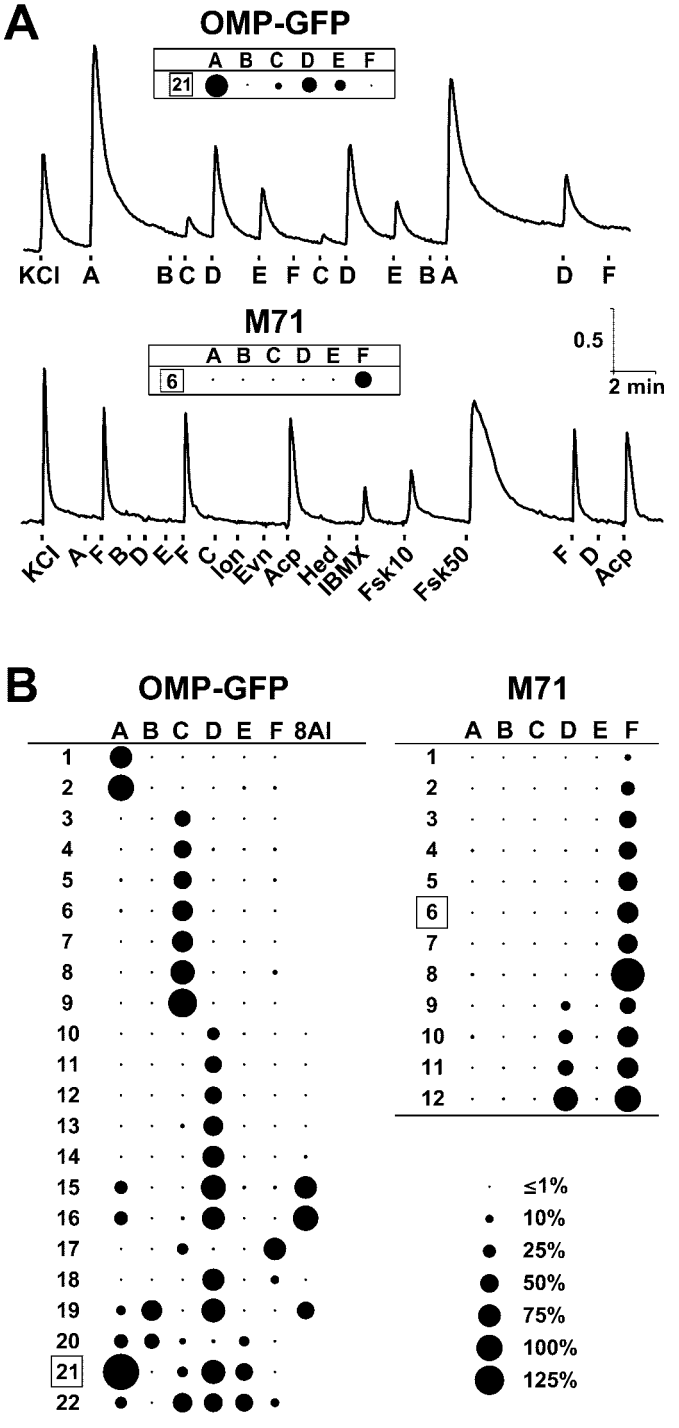

Figure 3. Similarity of response profiles to mixtures in M71 OSNs. *A*, Calcium imaging traces and corresponding dot plot response profiles from individual OSNs, OMP-GFP cell 21 (*top*), and M71-G cell 6 (*bottom*). Data are F_{340}/F_{380} ratios. *Marks* under the *traces* indicate 4 sec stimulus applications. All odorant concentrations were 25 μM. *KCl*, High K^+ Ringer's solution; *A–F*, mixes A–F; *Ion*, β-ionone; *Evn*, ethyl vanillin; *Acp*, acetophenone; *Hed*, hedione; *8Al*, octanal; *IBMX*, 500 μM IBMX; *Fsk10*, *Fsk50*, 10 and 50 μM forskolin. The *dot size* represents the amplitude of the calcium response to an odorant at 25 μM relative to the amplitude of the response to KCl. *B*, Plots for 22 individual OMP-GFP and 12 individual M71 OSNs tested with the odorant mixtures at 25 μM. Whereas a wide variety of response profiles is seen in randomly selected OSNs, a restricted set of profiles is found in M71 OSNs. Scale on the *bottom right* shows the size of *dots* corresponding to selected response amplitudes.

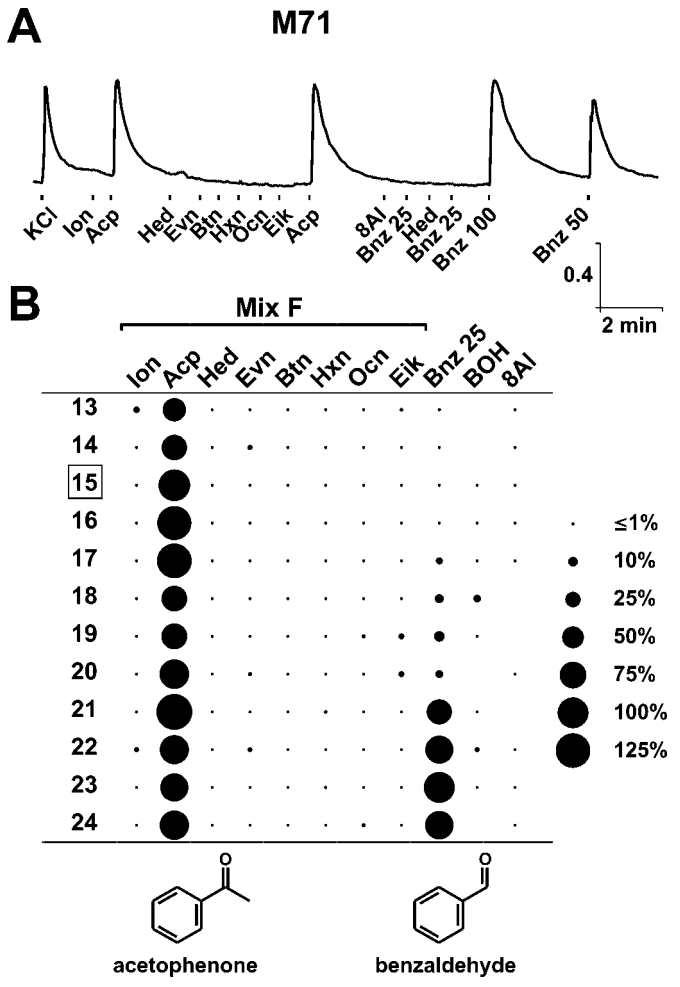

Figure 4. Identification of odorous agonists for M71. *A*, Calcium responses in an individual M71 OSN (*cell 15*) stimulated with individual mixture components. Odorant concentrations were 25 μM unless otherwise noted. *KCl*, high K^+ Ringer's solution; *Ion*, β-ionone; *Acp*, acetophenone; *Hed*, hedione; *Evn*, ethyl vanillin; *Btn*, butanone; *Hxn*, hexanone; *Oct*, octanone; *Eik*, ethyl isoamyl ketone; *Bnz25*, *Bnz50*, *Bnz100*, 25, 50, and 100 μM benzaldehyde; *BOH*, benzyl alcohol; *8Al*, octanal; *IBMX*, 500 μM IBMX; *Fsk10*, 10 μM forskolin. *B*, Response profiles for 12 individual M71 OSNs tested with mixture components at 25 μM. Responses are observed to the mix F component acetophenone and to the mix D component benzaldehyde. Absence of a *dot* indicates that the stimulus was not tested. Chemical structures for M71 agonists are shown (*bottom*).

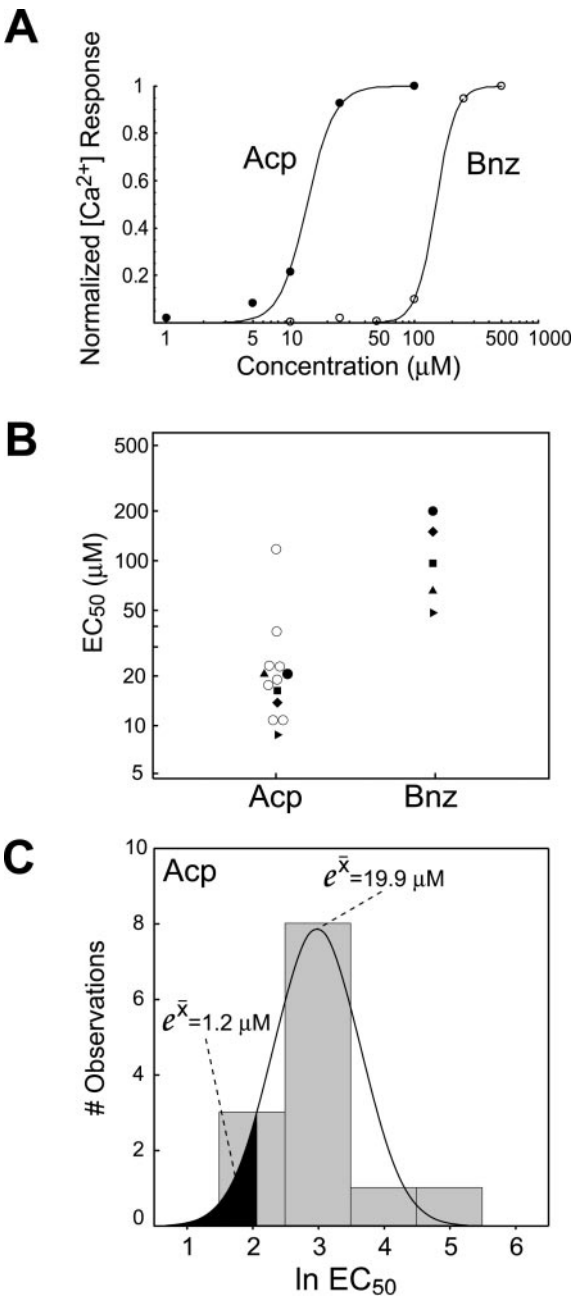

Figure 5. Dose–response relationships in M71 OSNs. *A*, Plot of calcium response versus odorant concentration for an M71 OSN to acetophenone (*Acp*; *filled circles*) and benzaldehyde (*Bnz*; *open circles*). *Continuous lines* represent best fits of the Hill equation to the normalized $[Ca^{2+}]$ response amplitudes. EC_{50} values for acetophenone and benzaldehyde for this cell are 14 and 150 μM, respectively. *B*, Plot of EC_{50} values obtained from 13 individual M71 OSNs. Each *data point* represents the EC_{50} for a single neuron. *Open circles* represent cells in which only the EC_{50} for acetophenone was determined. *Filled symbols* represent five neurons in which EC_{50} values were determined for both acetophenone and benzaldehyde in the same cell. *C*, Gaussian fit to the distribution of acetophenone EC_{50} values for M71 OSNs shown in *B*. The predicted mean EC_{50} for the most sensitive 10% of the neurons (*black area*) is 1.2 μM, >10-fold lower than the mean EC_{50} for the population as a whole.

responsive cells, 12 responded to at least one of the components at 25 μM (Fig. 4, *cells 13–24*). All 12 OSNs were stimulated by the mix F component acetophenone, whereas four (33%) also exhibited large calcium increases to the mix D component benzaldehyde. Large responses to other components were not observed; sporadic small deviations from baseline may represent movement artifacts or responses to low-affinity agonists for M71. Acetophenone-responsive OSNs that exhibited no response to benzaldehyde at 25 μM exhibited robust responses to this compound at 50 or 100 μM (four of four cells) (Fig. 4*A*).

The variability in the response amplitudes to acetophenone and benzaldehyde could result from differences in the relative sensitivity to the two odorants across neurons, with some cells being more sensitive to acetophenone and others being equally sensitive to both compounds. Alternately, the relative sensitivity to the two compounds could be fixed (i.e., the threshold for acetophenone is consistently lower than for benzaldehyde), but the overall sensitivity of the neurons may vary. Therefore, similarity of response profiles must be determined across concentration. A third set of 21 KCl-responsive M71 OSNs from 50 mice were tested with both

acetophenone and benzaldehyde at multiple concentrations, and dose–response relationships were determined. All 21 neurons responded to acetophenone at or above 25 μM, whereas 11 of 15 cells responded to benzaldehyde at or above 25 μM. Acetophenone dose–response curves were compiled for 13 OSNs; of these, benzaldehyde dose–response curves were compiled for five OSNs.

Dose–response relationships for $[Ca^{2+}]_i$ in M71 OSNs were steep, with threshold and saturation often falling within one log unit of stimulus concentration (Fig. 5*A*). The peak $[Ca^{2+}]$ response to odorants was 646 ± 87 nM (mean ± SEM; $n = 13$). The saturation of the odorant response was not likely attributable to saturation of fura-2 because the maximal odorant response amplitudes were frequently smaller than those evoked by KCl depolarization and were always smaller than the response amplitude elicited with the calcium ionophore ionomycin (data not shown).

The overall sensitivity of M71 OSNs to acetophenone varied over two orders of magnitude (Fig. 5*B*). The geometrical mean EC_{50} values for acetophenone and benzaldehyde were 19.9 μM ($n = 13$) and 98.4 μM ($n = 5$) respectively; this difference was statistically significant (paired-samples *t* test; $p < 0.001$). Individual neurons that responded to both compounds consistently exhibited a higher sensitivity to acetophenone than to benzaldehyde (Fig. 5*B*). Given the range of sensitivity observed for a single compound, the most sensitive 10% of a neuronal population with the observed mean and SD would exhibit a mean EC_{50} of 1.2 μM for acetophenone (Fig. 5*C*). Thus, a significant proportion of afferents projecting to a given glomerulus may exhibit a mean affinity that is ~10-fold higher than the afferent population as a whole.

Together, we thus identified a common odorant response profile in 37 individual M71 OSNs. Whereas the population as a whole responds over a wide range of stimulus concentrations, the individual neurons exhibit similar relative sensitivity across concentration with respect to acetophenone and benzaldehyde. It should be noted that, when responsiveness of neurons was tested across concentration, 21 of 21 OSNs (100%) responded to acetophenone, suggesting that a vast majority, if not all, M71 OSNs detect this odorant.

Functional similarity is mediated by M71

We demonstrated a tight correlation between expression of the *M71* gene and responsiveness to acetophenone and benzaldehyde. However, this correlation does not allow us to conclude that M71 mediates responses to one or both of these compounds, because M71 may be coexpressed with another OR or another molecule that itself would be responsible for the observed responses. To address this, we replaced the *M71* coding sequence with the rat *I7* OR coding sequence (Fig. 1*A*). Previous studies had identified octanal and related aliphatic aldehydes as ligands for rat I7 (Krautwurst et al., 1998; Zhao et al., 1998). Thus, we reasoned that the rI7→M71 coding sequence swap should result in a loss of responsiveness to acetophenone and benzaldehyde and a gain of responsiveness to expected rat I7 agonists such as octanal.

A set of 43 KCl-responsive rI7→M71 OSNs from 50 mice were stimulated with the odorant mixtures and/or individual components. Four cells responded to forskolin only, and 25 responded to at least one odorant stimulus at 25 μM. Of these, 15 OSNs were tested repeatedly with odorants and were included in the analysis (Fig. 6*B*, *cells 1–15*). In contrast to M71 OSNs, responses could be elicited in rI7→M71 OSNs using mix D and mix A but not mix F (Fig. 6*A*). All neurons tested responded to octanal ($n = 15$), although none responded to acetophenone or benzaldehyde ($n = 13$) (Fig. 6*B*), even at 100 μM (data not shown). Conversely, responses to octanal were not observed in M71 OSNs ($n = 9$) (Fig. 4*B*). Thus, M71 mediates the responses to both acetophenone and benzaldehyde.

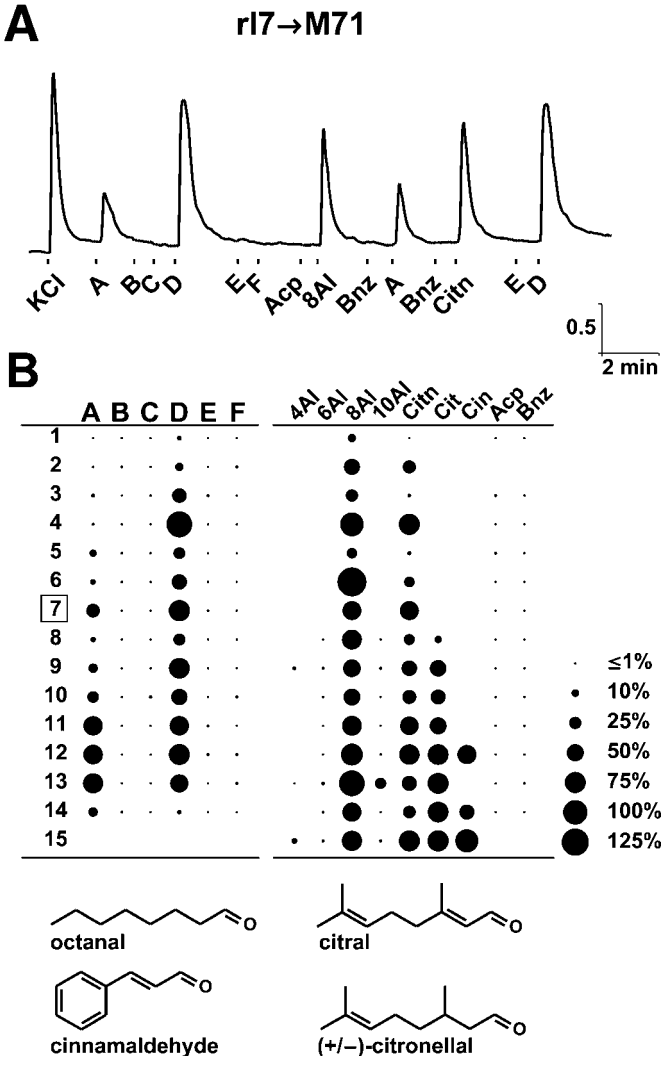

Figure 6. Odorant response profiles of rI7→M71 OSNs. *A*, Calcium responses in a single rI7→M71 OSN (*cell 7*) stimulated with the odorant mixtures and selected components at 25 μM. *B*, Response profiles for 15 individual rI7→M71 OSNs tested with mixtures (*left*) and components (*right*) at 25 μM. Neurons responded to octanal, citronellal, citral, and cinnamaldehyde but not to acetophenone and benzaldehyde. Absence of a *dot* indicates that the odorant was not tested. *KCl*, High K^+ Ringer's solution; *A–F*, mixes A–F; *4Al*, butanal; *6Al*, hexanal; *8Al*, octanal; *10Al*, decanal; *Citn*, (+)- and (−)-citronellal; *Cit*, citral; *Cin*, cinnamaldehyde; *Acp*, acetophenone; *Bnz*, benzaldehyde. Chemical structures for rI7→M71 agonists are shown (*bottom*).

In our assay, the response profiles observed for the rat I7 OR are similar to those reported previously (Krautwurst et al., 1998; Zhao et al., 1998; Araneda et al., 2000), albeit with some differences. Consistent with previous findings, rI7→M71 OSNs responded to the mix A component citronellal and failed to respond to butanal ($n = 3$) and hexanal ($n = 8$). In our assay, only one of eight neurons was stimulated by decanal, a compound that has been reported as a rat I7 agonist (Araneda et al., 2000). Moreover, robust responses were seen to cinnamaldehyde (three of three cells), which has not been identified as an I7 agonist, and to

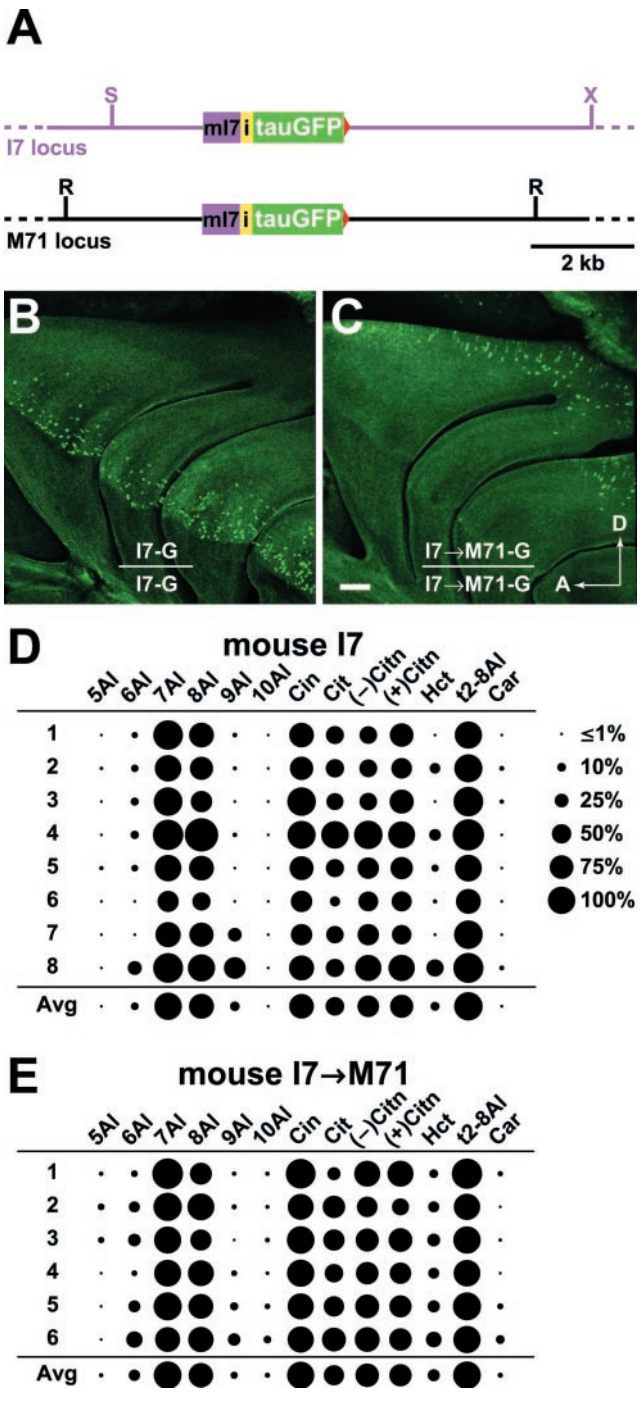

Figure 7. Response profiles of mouse I7 expressed in different zones. *A*, *Top*, Diagram of the (*mI7-IRES-tauGFP*) allele. *IRES-tauGFP* (*green box*) sequences are inserted just after the mouse *I7* coding sequence (*purple box*) in the endogenous mouse *I7* locus (*purple line*). *Bottom*, Diagram of the *mI7→M71-IRES-tauGFP* allele. The mouse *I7* coding sequence (*purple box*) and *IRES-tauGFP* sequences replace the M71 coding sequence in the *M71* locus (*black line*). Both alleles are illustrated after Cre-mediated excision of the *neo*-selectable markers. *B*, View of the medial face of the turbinates in an I7-G mouse showing GFP-labeled neurons in the most ventral zone (zone 1) of the olfactory epithelium. *C*, View of the medial turbinates in an I7→M71-G mouse showing GFP-labeled neurons in the most dorsal zone of the olfactory epithelium (zone 4). Response profiles for eight mouse I7 neurons (*D*) and six mI7→M71 OSNs (*E*) tested with a homologous series of aldehydes at 25 μM. Neurons from both strains exhibited similar response profiles. Large responses were elicited by heptanal, octanal, cinnamaldehyde, (+)-citronellal, (−)-citronellal, citral, and *trans*-2-octenal. Average responses (*Avg*) are shown at the *bottom* of each plot. *5Al*, Pentanal; *6Al*, hexanal; *7Al*, heptanal; *8Al*, octanal; *9Al*, nonanal; *10Al*, decanal; *Cin*, cinnamaldehyde; *Citn*, citronellal; *Cit*, citral; *Hct*, hydroxycitronellal; *t2–8Al*, *trans*-2-octenal; *Acp*, acetophenone; *Car*, (+)- and (−)-carvone.

citral (eight of eight cells), which has been characterized as a partial agonist for rat I7 (Zhao et al., 1998; Araneda et al., 2000). In many rI7→M71 OSNs, responses to these odorants were equal in amplitude to responses elicited with octanal.

Interzonal swap of mouse I7

The discrepancy observed in the agonist profiles for rI7→M71 may be caused by gross changes in odorant response properties attributable to expression in different species (rat vs mouse) or in different zones within a species (rat I7 in zone 1, M71 in zone 4). We tested the latter possibility by comparing the response properties of OSNs expressing the mouse *I7* gene from its endogenous locus with OSNs expressing mouse I7 from the M71 locus (mI7→M71). The mouse I7 OR differs in 15 amino acid residues from rat I7 and is reported to have slightly different response properties (Chess et al., 1994; Krautwurst et al., 1998; Zhao et al., 1998). We targeted the endogenous mouse *I7* gene with tauGFP (*mI7-IRES-tauGFP*) and swapped the mouse I7 coding sequence into the M71 locus (*mI7→M71-IRES-tauGFP*) (Fig. 7*A*). The mouse *I7* gene is expressed in the most ventral zone (zone 1) of the olfactory epithelium (Fig. 7*B*), whereas the mI7→M71 swap is expressed in the most dorsal zone (zone 4), as seen in rI7→M71 mice (compare Figs. 1*C*, 7*C*). We then tested for differences in response profiles using a homologous series of aldehydes, including identified rat I7 agonists.

Neurons from both mouse I7 strains exhibited robust responses to the known rat I7 agonists heptanal, octanal, *trans*-2-octenal, and both (+) and (−) isomers of citronellal. The mouse I7 OR has been reported to respond to heptanal but not octanal at a single concentration (Krautwurst et al., 1998). We observed that both compounds were effective stimuli at 25 μM. Similar to rI7→M71, robust responses were also observed to cinnamaldehyde and citral in both strains. The smaller, sporadic responses to hexanal, nonanal, and hydroxycitronellal in both mouse I7 strains are similar to benzaldehyde responses seen in M71 OSNs (Fig. 4*B*). This suggests that responses to these ligands may be near the threshold of detection in our assay at 25 μM. The similarity of the two population responses strongly suggests that zone of expression does not drastically alter the specificity of mouse I7 for the tested odorants. It also indicates that zone of expression does not explain the subtle differences observed in the rat I7 response profile.

Axonal projections of M71 and rI7→M71 OSNs

ORs are known to play a role in axon guidance, because swapping the OR at a given locus changes the location of glomerular formation. Axons from M71 OSNs project the caudal aspect of the dorsal OB (Fig. 8*A*). When expressing rat I7, however, the location of axonal convergence shifts anteriorly (Fig. 8, compare *A*, *B*). To determine the extent of the axonal rerouting within the same mouse, we crossed homozygous M71-G mice to homozygous rI7→M71-G mice, thus creating compound heterozygotes at the *M71* locus. Because of monoallelic expression of OR genes (Chess et al., 1994; Strotmann et al., 2000; Ishii et al., 2001), one-half of the OSNs expressing the M71 locus should express M71 and tauGFP, whereas one-half should express rat I7, GFP,

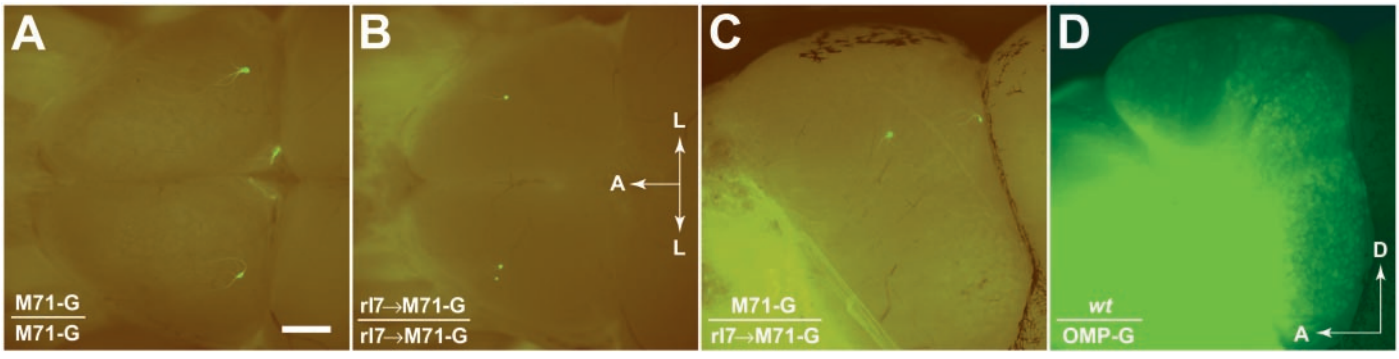

Figure 8. Shifted glomerular position in rI7→M71 mice. *A*, *B*, Dorsal view of the left and right OBs from a homozygous M71-G mouse (*A*) and from a homozygous rI7→M71-G mouse (*B*) showing the bilaterally symmetrical location of the lateral glomeruli in the dorsal OB. The *horizontal arrow* in *B* marks the midline of the mouse; *right* is above, and *left* is below. Out-of-focus fluorescence from the medial glomeruli can also be seen in M71-G mice (*A*). Note the presence of a double lateral glomerulus in the left (*bottom*) OB in *B*. *C*, Medial view of the right OB from a M71-G × rI7→M71-G compound heterozygous mouse in which labeled rI7→M71 (*left*) and M71 (*right*) glomeruli form in the same mouse. The resulting glomeruli are smaller and less bright than those from homozygous M71-G and rI7→M71-G mice, consistent with the fact that approximately one-half of the number of axons converge to each glomerulus. The rat I7 swap shifts the site of axonal convergence anterior and ventral with respect to M71. *D*, Medial view of the right OB from a heterozygous OMP-GFP mouse in which all glomeruli are labeled. *A*, Anterior; *L*, lateral; *D*, dorsal; *wt*, wild type. Scale bar, 650 μm.

and taulacZ. Consequently, GFP-expressing axons should segregate into two populations based on OR expression, resulting in the formation of separate glomeruli, each comprising approximately one-half the number of afferents. Consistent with this idea, two glomeruli can be seen on the medial (Fig. 8*C*) and lateral (data not shown) hemispheres of the OB in compound heterozygous mice; as expected, these glomeruli are smaller in size and less intensely fluorescent than in homozygous mice (data not shown). The rat I7 swap results in axonal rerouting to a more anterior, ventral position. Axons from rI7→M71 OSNs, which can be distinguished from M71 axons by X-gal staining, do not project to the M71 glomeruli ($n = 6$ mice; data not shown), indicating that all rI7→M71 axons are rerouted.

Neurons that express the *M71* gene typically project to a single medial and single lateral glomerulus in the dorsal OB (Fig. 8*A*). However, both M71 and rI7→M71 OSNs occasionally form multiple glomeruli in each hemisphere of the OB (Fig. 8*B*, left bulb). Interestingly, the frequency of multiple glomeruli was different in the two strains. For M71, 14% of medial and lateral convergent loci examined exhibited double glomeruli ($n = 118$ sites); 6 of 22 mice (27%), in which all four convergent loci were viewed, exhibited at least one double glomerulus. For rI7→M71, 34% of convergence sites had two glomeruli, and 3% had three glomeruli ($n = 102$ sites); 21 of 26 (81%) mice examined exhibited multiple glomeruli in at least one medial or lateral convergence site. The incidence of multiple glomeruli is significantly different between the two strains (χ^2 test; $p < 0.001$). Thus, the formation of multiple glomeruli correlates with the expressed OR coding sequence and not with the locus of expression in a defined neuronal population.

Mouse *I7* is normally expressed by neurons in the most ventral zone of the olfactory epithelium. When swapped into the *M71* locus, expression of both rat and mouse I7 ORs is imposed in OSNs whose cell bodies reside in the most dorsal epithelial zone. Because the zones project globally onto distinct regions in the OB (Mori et al., 1999), it is not surprising that the rI7→M71 glomeruli are at a considerable distance from the endogenous mouse I7 glomeruli, which are located in the ventral OB (data not shown).

To examine whether rI7→M71 OSNs innervate a glomerulus with another afferent population or form novel glomeruli, we looked for nontagged axons within rI7→M71 glomeruli in homozygous mice by labeling all afferents with an antibody to the G-protein subunit $G_{\alpha olf}$ (G_{olf}). In control experiments, staining for G_{olf} in M71-G heterozygous mice reveals nontagged axons within M71 glomeruli (Fig. 9*A*); by inference, the nontagged axons are from OSNs that express the wild-type *M71* allele. Thus, this method can detect nontagged axons within a labeled glomerulus, as demonstrated for P2 glomeruli (Belluscio et al., 1999). In contrast, glomeruli in homozygous rI7→M71 mice (Fig. 9*C*) are indistinguishable from those in homozygous M71-G mice (Fig. 9*B*), demonstrating that a majority of axons projecting to rI7→M71 glomeruli are GFP tagged and thus express rat I7. This suggests that expression of the exogenous rat I7 OR directs afferents to form novel glomeruli that are homogeneously innervated by this novel OSN population.

DISCUSSION

We used a combination of gene targeting and calcium imaging to functionally analyze OSNs that express defined ORs. This method has revealed previously unknown agonists for M71, rat I7, and mouse I7 ORs. Our results demonstrate that expression of

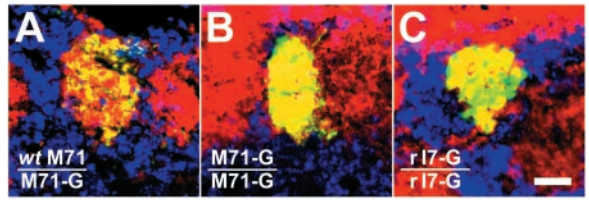

Figure 9. Formation of novel glomeruli by rI7→M71 OSNs. *A*, Cross-section through an M71 glomerulus in a heterozygous M71-G mouse. After staining with an antibody against G_{olf} (*red*) to label all afferents, GFP-tagged (GFP^+) axons are *green* and *red* (*yellow*), and nontagged (GFP^-) axons are only *red*. GFP^+ and GFP^- axons can be visualized in the same section when a glomerulus receives inputs from a mixed population of OSNs. *B*, The same experiment in homozygous M71-G mice shows that the M71 glomerulus receives most or all of its input from GFP^+–$G_{olf}{}^+$ (*yellow*) axons. *C*, The pattern of labeling in an rI7→M71 glomerulus in a homozygous rI7→M71-G mouse is indistinguishable from a homozygous M71 glomerulus and exhibits a preponderance of GFP^+–$G_{olf}{}^+$ (*yellow*) axons, indicating that these axons form novel glomeruli. All sections were counterstained with the nuclear dye TOTO-3 (*blue*). Scale bar, 25 μm.

a given OR imparts functional similarity to populations of OSNs while concomitantly directing the site of axonal convergence in the OB. Moreover, expressing a given OR in different zones of the olfactory epithelium did not significantly alter the observed response profiles. Our data confirm and extend the notion that the expressed OR directs the functional organization of the primary olfactory projection, resulting in glomeruli that receive inputs from functionally similar afferents.

OR agonist profiles

Previous studies have associated ligands with vertebrate ORs using single-cell PCR (Malnic et al., 1999; Touhara et al., 1999; Kajiya et al., 2001), *in vitro* heterologous expression (Krautwurst et al., 1998; Wetzel et al., 1999), and *in vivo* overexpression assays (Zhao et al., 1998; Araneda et al., 2000). It is important to determine whether ligand profiles determined using these methods hold true in native OSNs. The present study permits us to examine, for the first time, the response properties of defined ORs expressed from endogenous genetic loci and coupled to appropriate second-messenger pathways in olfactory cilia.

Using this assay, we confirm certain aspects of the reported rat and mouse I7 response profiles (Krautwurst et al., 1998; Zhao et al., 1998; Araneda et al., 2000) but observe differences in others. We find that mouse and rat I7 both respond to cinnamaldehyde and citral, agonists not previously associated with either OR, whereas decanal did not elicit responses in all rI7→M71 OSNs at the single concentration tested. These differences are not likely caused by the zone of expression because mouse I7 behaves similarly when expressed in two distinct zones in the mouse olfactory epithelium. Unfortunately, it is difficult to eliminate the possibility that rat I7 assumes a different ligand specificity when overexpressed in the rat or in heterologous systems. However, we believe it is more likely that the discrepancies are attributable to methodological factors such as relative concentration of odorants, method of stimulus delivery, levels of OR expression, and/or type of assay (field potentials in whole epithelium vs calcium imaging in single cells). Our findings point out the necessity to compare data from different assays to assess the response properties of ORs.

Dynamic range of OSNs

Odorant-induced calcium responses in M71 OSNs saturate over an ~10-fold increase in stimulus concentration. This is similar to the dynamic range observed when measuring transduction current and/or spike frequency in randomly selected OSNs *in vitro* (Firestein et al., 1993; Reisert and Matthews, 1999). Although calcium transients in the cilia correlate with transduction current in amphibian OSNs (Reisert and Matthews, 2001), the degree to which somatic $[Ca^{2+}]_i$ accurately reflects transduction current or spike frequency is not known; somatic Ca^{2+} transients likely result from voltage-gated Ca^{2+} channel activation (Schild et al., 1994) and Ca^{2+}-induced Ca^{2+} release (Zufall et al., 2000). Despite this, calcium imaging revealed a consistent differential sensitivity of the M71 OR to particular odorants (acetophenone and benzaldehyde), indicating that this method accurately reports relative odorant responsiveness resulting from underlying OR expression.

Sensitivity of odorant responses

Single-cell thresholds obtained in our experiments and in published physiological studies are often several orders of magnitude higher than behavioral thresholds observed in animals (Reisert and Matthews, 1999; Duchamp-Viret et al., 2000; Reisert and Matthews, 2001). This apparent lack of sensitivity may result from factors unrelated to the health or state of the cells. First, detection thresholds in animals result from the sensitivity of the individual OSNs, as well as circuit properties (convergence, amplification, and noise reduction) of the olfactory pathway. It is possible that intact animals can exhibit behavioral thresholds well below the EC_{50} of its sensors. Second, afferents that innervate a glomerulus may exhibit a range of sensitivities, as shown by our data. Some proportion of these OSNs would be significantly more sensitive than the mean EC_{50} of the population (Cleland and Linster, 1999; Wachowiak and Cohen, 2001).

Third, behavioral thresholds for the odorants used in our assay (e.g., acetophenone) are likely determined by ORs with higher affinities than the ORs studied here (e.g., M71). The response breadth of OSNs has been shown to narrow with decreasing concentration (Sato et al., 1994), suggesting that ORs respond to some set of low-affinity agonists and a relatively more restricted subset of high-affinity agonists. If this is true, the probability of encountering a high-affinity agonist may be low. Despite this, two effective stimuli (acetophenone and benzaldehyde) were identified when subjecting a single odorant receptor (M71) to a test panel of 48 compounds at relatively high concentrations. A similar case can be made for rat I7 (although octanal was included as an odorant given a priori knowledge of the I7 response spectrum) because the odorant panel contained two previously unidentified I7 agonists (citronellal and cinnamaldehyde). The most likely explanation for the high proportion of effective stimuli is that the identified odorants are relatively low-affinity agonists. Viewed in this way, the reproducible and selective response profiles observed in genetically identified neurons are consistent with broad tuning of individual mouse OSNs (Duchamp-Viret et al., 1999) and anatomically identified mouse glomeruli (Wachowiak and Cohen, 2001).

Differences in overall sensitivity among neurons likely contributed to the variability observed in response profiles determined at a single concentration; this effect would be exacerbated by the steep dose–response relationships observed. Stimulus sensitivity may be affected by variation in OR expression level, modulation of signal transduction pathways (Schild and Restrepo, 1998), differential expression of auxiliary proteins that may effect ligand binding (McLatchie et al., 1998), or differences in spare-receptor capacity (Cleland and Linster, 1999). However, we cannot rule out that variable sensitivity resulted from alterations in cell morphology or physiology caused by dissociation (e.g., number of intact cilia or proximity of dendritic knob to cell soma). To address this issue, we are developing methods to examine responses from genetically defined OSNs in more intact preparations. If the variability in EC_{50} values observed in dissociated OSNs is also observed *in vivo*, afferents innervating a given glomerulus that share similar tuning profiles may respond over different concentration ranges. This provides a potential explanation for the broad dynamic range of afferent input to defined glomeruli (Friedrich and Korsching, 1997; Wachowiak and Cohen, 2001).

Relationship between ORs and glomeruli

Our data provide compelling evidence that OR expression defines parallel information pathways, each consisting of a population of sensory neurons that share similar functional properties. Electron microscopic analysis of gene-targeted mice demonstrates that axons from OSNs expressing the same OR converge to form mutually exclusive glomeruli (Treloar et al., 2002). Thus, OR expression determines the formation of glomeruli that are

functional units at the level of afferent input. However, we also observe that axons from OR-defined OSNs occasionally form multiple glomeruli; similar data have been shown for the ORs P2, mOR37, and M72 in gene-targeted mice (Royal and Key, 1999; Strotmann et al., 2000; Zheng et al., 2000) and for M50 in wild-type mice (Lin et al., 2000). This is consistent with subtle bilateral asymmetries in odorant response patterns observed in the rodent OB (Johnson et al., 1999; Rubin and Katz, 1999; Belluscio and Katz, 2001; Meister and Bonhoeffer, 2001). Thus, the glomerular representation of functionally similar OSN populations may vary, and all glomeruli that receive mutually exclusive inputs from these OSNs should be considered part of a functional unit.

Expression of the rat *I7* coding sequence from the *M71* locus results in a significantly higher incidence of multiple glomeruli than expression of the *M71* coding sequence. This suggests that the probability of forming multiple glomeruli, which occurs with wild-type alleles (Lin et al., 2000), likely relates to which OR protein is expressed. The formation of multiple glomeruli may be affected by the position of glomerular convergence on the OB surface, the total number of OSNs expressing a given OR, or variability in the level of OR expression within a defined neuronal population.

The present data are consistent with the notion that ORs mediate both axon guidance (Mombaerts et al., 1996; Wang et al., 1998) and odorant responsiveness. Interestingly, when rat *I7* is expressed in the mouse, it directs the formation of novel glomeruli that do not exist in nongenetically manipulated mice. This reveals a plasticity in the glomerular array that may reflect the evolutionary imperative to form a novel glomerulus when a novel OR gene or allelic variant emerges. Determining to what degree the formation of novel glomeruli correlates with changes in odor specificity will provide insight into the logic of stimulus mapping in the OB.

REFERENCES

Araneda RC, Kini AD, Firestein S (2000) The molecular receptive range of an odorant receptor. Nat Neurosci 3:1248–1255.

Belluscio L, Katz LC (2001) Symmetry, stereotypy, and topography of odorant representations in mouse olfactory bulbs. J Neurosci 21:2113–2122.

Belluscio L, Koentges G, Axel R, Dulac C (1999) A map of pheromone receptor activation in the mammalian brain. Cell 97:209–220.

Bozza TC, Kauer JS (1998) Odorant response properties of convergent olfactory receptor neurons. J Neurosci 18:4560–4569.

Brand A (1995) GFP in *Drosophila*. Trends Genetics 11:324–325.

Buck L, Axel R (1991) A novel multigene family may encode odorant receptors: a molecular basis for odor recognition. Cell 65:175–187.

Buiakova OI, Baker H, Scott JW, Farbman A, Kream R, Grillo M, Franzen L, Richman M, Davis LM, Abbondanzo S, Stewart CL, Margolis FL (1996) Olfactory marker protein (OMP) gene deletion causes altered physiological activity of olfactory sensory neurons. Proc Natl Acad Sci USA 93:9858–9863.

Bunting M, Bernstein KE, Greer JM, Capecchi MR, Thomas KR (1999) Targeting genes for self-excision in the germ line. Genes Dev 13:1524–1528.

Chess A, Simon I, Cedar H, Axel R (1994) Allelic inactivation regulates olfactory receptor gene expression. Cell 78:823–834.

Cleland TA, Linster C (1999) Concentration tuning mediated by spare receptor capacity in olfactory sensory neurons: a theoretical study. Neural Comput 11:1673–1690.

Duchamp-Viret P, Chaput MA, Duchamp A (1999) Odor response properties of rat olfactory receptor neurons. Science 284:2171–2174.

Duchamp-Viret P, Duchamp A, Chaput MA (2000) Peripheral odor coding in the rat and frog: quality and intensity specification. J Neurosci 20:2383–2390.

Firestein S, Picco C, Menini A (1993) The relation between stimulus and response in olfactory receptor cells of the tiger salamander. J Physiol (Lond) 468:1–10.

Friedrich RW, Korsching SI (1997) Combinatorial and chemotopic odorant coding in the zebrafish olfactory bulb visualized by optical imaging. Neuron 18:737–752.

Frings S, Lindemann B (1991) Current recording from sensory cilia of olfactory receptor cells in situ. I. The neuronal response of cyclic nucleotides. J Gen Physiol 97:1–16.

Grynkiewicz G, Poenie M, Tsien RY (1985) A new generation of Ca^{2+} indicators with greatly improved fluorescence properties. J Biol Chem 260:3440–3450.

Hildebrand JG, Shepherd GM (1997) Mechanisms of olfactory discrimination: converging evidence for common principles across phyla. Annu Rev Neurosci 20:595–631.

Ishii T, Serizawa S, Kohda A, Nakatani H, Shiroishi T, Okumura K, Iwakura Y, Nagawa F, Tsuboi A, Sakano H (2001) Monoallelic expression of the odourant receptor gene and axonal projection of olfactory sensory neurones. Genes Cells 6:71–78.

Johnson BA, Woo CC, Hingco EE, Pham KL, Leon M (1999) Multidimensional chemotopic responses to n-aliphatic acid odorants in the rat olfactory bulb. J Comp Neurol 409:529–548.

Kajiya K, Inaki K, Tanaka M, Haga T, Kataoka H, Touhara K (2001) Molecular bases of odor discrimination: reconstitution of olfactory receptors that recognize overlapping sets of odorants. J Neurosci 21:6018–6025.

Kao JPY (1994) Practical aspects of measuring $[Ca^{2+}]$ with fluorescent indicators. Methods Cell Biol 40:155–181.

Kauer JS (1987) Coding in the olfactory system. In: Neurobiology of taste and smell (Finger TE, Silver WL, eds), pp 205–231. New York: Wiley.

Kauer JS, Cinelli AR (1993) Are there structural and functional modules in the vertebrate olfactory bulb? Microsc Res Tech 24:157–167.

Krautwurst D, Yau KW, Reed RR (1998) Identification of ligands for olfactory receptors by functional expression of a receptor library. Cell 95:917–926.

Lakso M, Pichel JG, Gorman JR, Sauer B, Okamoto Y, Lee E, Alt FW, Westphal H (1996) Efficient in vivo manipulation of mouse genomic sequences at the zygote stage. Proc Natl Acad Sci USA 93:5860–5865.

Leinders-Zufall T, Rand MN, Shepherd GM, Greer CA, Zufall F (1997) Calcium entry through cyclic nucleotide-gated channels in individual cilia of olfactory receptor cells: spatiotemporal dynamics. J Neurosci 17:4136–4148.

Lin DM, Wang F, Lowe G, Gold GH, Axel R, Ngai J, Brunet L (2000) Formation of precise connections in the olfactory bulb occurs in the absence of odorant-evoked neuronal activity. Neuron 26:69–80.

Malnic B, Hirono J, Sato T, Buck LB (1999) Combinatorial receptor codes for odors. Cell 96:713–723.

McLatchie LM, Fraser NJ, Main MJ, Wise A, Brown J, Thompson N, Solari R, Lee MG, Foord SM (1998) RAMPs regulate the transport and ligand specificity of the calcitonin-receptor-like receptor. Nature 393:333–339.

Meister M, Bonhoeffer T (2001) Tuning and topography in an odor map on the rat olfactory bulb. J Neurosci 21:1351–1360.

Mombaerts P (1999) Molecular biology of odorant receptors in vertebrates. Annu Rev Neurosci 22:487–509.

Mombaerts P, Wang F, Dulac C, Chao SK, Nemes A, Mendelsohn M, Edmondson J, Axel R (1996) Visualizing an olfactory sensory map. Cell 87:675–686.

Mori K, Nagao H, Yoshihara Y (1999) The olfactory bulb: coding and processing of odor molecule information. Science 286:711–715.

Murrell JR, Hunter DD (1999) An olfactory sensory neuron line, odora, properly targets olfactory proteins and responds to odorants. J Neurosci 19:8260–8270.

Potter SM, Zheng C, Koos DS, Feinstein P, Fraser SE, Mombaerts P (2001) Structure and emergence of specific olfactory glomeruli in the mouse. J Neurosci 21:9713–9723.

Reisert J, Matthews HR (1999) Adaptation of the odour-induced response in frog olfactory receptor cells. J Physiol (Lond) 519:801–813.

Reisert J, Matthews HR (2001) Simultaneous recording of receptor current and intraciliary Ca^{2+} concentration in salamander olfactory receptor cells. J Physiol (Lond) 535:637–645.

Ressler KJ, Sullivan SL, Buck LB (1993) A zonal organization of odorant receptor gene expression in the olfactory epithelium. Cell 73:597–609.

Ressler KJ, Sullivan SL, Buck LB (1994) Information coding in the olfactory system: evidence for a stereotyped and highly organized epitope map in the olfactory bulb. Cell 79:1245–1255.

Rodriguez I, Feinstein P, Mombaerts P (1999) Variable patterns of axonal projections of sensory neurons in the mouse vomeronasal system. Cell 97:199–208.

Royal SJ, Key B (1999) Development of P2 olfactory glomeruli in P2-internal ribosome entry site-tau-LacZ transgenic mice. J Neurosci 19:9856–9864.

Rubin BD, Katz LC (1999) Optical imaging of odorant representations in the mammalian olfactory bulb. Neuron 23:499–511.

Sato T, Hirono J, Tonoike M, Takebayashi M (1994) Tuning specificities to aliphatic odorants in mouse olfactory receptor neurons and their local distribution. J Neurophysiol 72:2980–2989.

Schild D, Restrepo D (1998) Transduction mechanisms in vertebrate olfactory receptor cells. Physiol Rev 78:429–466.

Schild D, Jung A, Schultens HA (1994) Localization of calcium entry through calcium channels in olfactory receptor neurones using a laser scanning microscope and the calcium indicator dyes Fluo-3 and Fura-red. Cell Calcium 15:341–348.
Strotmann J, Conzelman S, Beck A, Feinstein P, Breer H, Mombaerts P (2000) Local permutations in the glomerular array of the mouse olfactory bulb. J Neurosci 15:6927–6938.
Touhara K, Sengoku S, Inaki K, Tsuboi A, Hirono J, Sato T, Sakano H, Haga T (1999) Functional identification and reconstitution of an odorant receptor in single olfactory neurons. Proc Natl Acad Sci USA 96:4040–4045.
Treloar HB, Feinstein P, Mombaerts P, Greer CA (2002) Specificity of glomerular targeting by olfactory sensory axons. J Neurosci 22, in press.
Vassar R, Ngai J, Axel R (1993) Spatial segregation of odorant receptor expression in the mammalian olfactory epithelium. Cell 74:309–318.
Vassar R, Chao SK, Sitcheran R, Nuñez JM, Vosshall LB, Axel R (1994) Topographic organization of sensory projections to the olfactory bulb. Cell 79:981–991.
Wachowiak M, Cohen LB (2001) Representation of odorants by receptor neuron input to the mouse olfactory bulb. Neuron 32:723–735.
Wang F, Nemes A, Mendelsohn M, Axel R (1998) Odorant receptors govern the formation of a precise topographic map. Cell 93:47–60.
Wetzel CH, Oles M, Wellerdieck C, Kuczkowiak M, Gisselmann G, Hatt H (1999) Specificity and sensitivity of a human olfactory receptor functionally expressed in human embryonic kidney 293 cells and *Xenopus laevis* oocytes. J Neurosci 19:7426–7433.
Wong S, Trinh K, Hacker B, Chan G, Lowe G, Gaggar A, Xia Z, Gold G, Storm D (2000) Disruption of the type III adenylyl cyclase gene leads to peripheral and behavioral anosmia in transgenic mice. Neuron 27:487–497.
Xie SY, Feinstein P, Mombaerts P (2000) Characterization of a cluster comprising approximately 100 odorant receptor genes in mouse. Mamm Genome 11:1070–1078.
Zhang X, Firestein S (2002) The olfactory receptor gene superfamily of the mouse. Nat Neurosci 5:124–133.
Zhao H, Ivic L, Otaki JM, Hashimoto M, Mikoshiba K, Firestein S (1998) Functional expression of a mammalian odorant receptor. Science 279:237–242.
Zheng C, Feinstein P, Bozza T, Rodriguez I, Mombaerts P (2000) Peripheral olfactory projections are differentially affected in mice deficient in a cyclic nucleotide-gated channel subunit. Neuron 26:81–91.
Zufall F, Leinders-Zufall T, Greer CA (2000) Amplification of odor-induced Ca^{2+} transients by store-operated Ca^{2+} release and its role in olfactory signal transduction. J Neurophysiol 83:501–512.